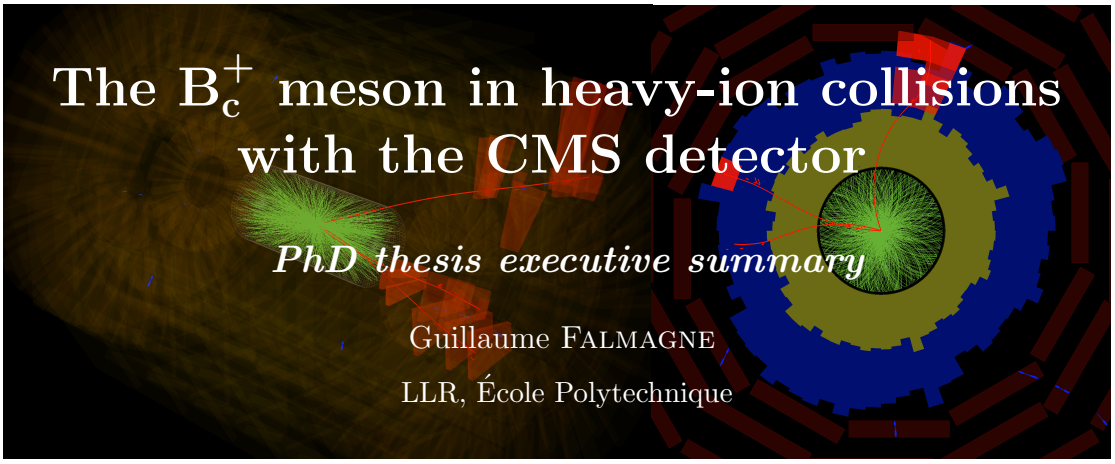

Figure 1: Display of the PbPb 2018 collision event #209030061 (run #327004) in the CMS detector, at a 5% centrality. *Left:* 3D view; *right:* transverse view. This event has a very high probability to contain a B_c meson decay to three muons, shown in red.

The strong interaction, at play in the nucleons composing atomic nuclei, is ruled by quantum chromodynamics (QCD). At high temperatures and densities, a rapid transition leads to an atypical regime of QCD: a state of matter called the quark-gluon plasma (QGP). The QGP is a close-to-perfect fluid of partons, produced at RHIC and LHC accelerators at temperatures higher than any current astrophysical process ($T \gg 10^{12}$ K). It was present in the first microseconds after the Big Bang and might constitute the core of neutron stars today. Asymptotic freedom weakens the strong interaction at small distances; while at larger distances, the colour charge is confined and hadrons start to form. This colour confinement phenomenon is yet poorly understood. What are the relevant QCD degrees of freedom: quarks, gluons, or hadrons such as the protons and neutrons we are made of? How do quarks hadronise, and how are these processes modified in a hot QCD-coloured medium? Studying the QGP, in which coloured particles (i.e. partons such as quarks and gluons) roam freely, can help address these standing questions.

The lead-lead (PbPb) collisions at the LHC at CERN create a QGP, that can be studied via its impact on the production of the detected final-state particles. To that goal, the nuclear modification factor R_{AA} is often used, i.e. the production yields in heavy ion (AA) collisions compared to the normalised yields in proton-proton (pp) collisions, where no QGP is produced.

This thesis addresses how high-energy partons and the hadronisation of heavy quarks (charm c and bottom b) are affected by the QGP in lead-lead (PbPb) collisions at the LHC. Data from the CMS detector are analysed to achieve the **first observation of B_c^+ mesons in heavy-ion collisions** (charge conjugated states are implied throughout). The B_c^+ meson cross sections in pp and PbPb and its nuclear modification factor $R_{\mathrm{PbPb}}(B_c^+)$ are measured in two bins of the visible transverse momentum and of the PbPb collision centrality. The now-published results [1] notably show a smaller suppression for B_c than for other hadrons, which points to the importance of heavy quark recombination processes in the hot medium. A phenomenology work is also presented, treating how high-energy partons lose energy when traversing the QGP. An existing model of **radiative energy loss in the medium** predicts a universal p_{T} shape for the R_{AA} of high-p_{T} hadrons [2], which is confirmed in this thesis using more measurements than the original work, from collision systems of broadly different characteristics [3]. The mean energy loss values extracted from these many systems are also found to scale with the multiplicity and geometry of the event. The resulting **constraints on the expansion of the medium** hold when varying the Glauber model (including with custom ones) used to describe the AA collision event.

The Standard Model of particle physics, its strong interaction and QCD, and basics of the QGP, are introduced in Chapter 1. In Chapter 2, the search for B_c^+ mesons in heavy ion collisions is motivated by explaining how it bridges the gap between charmonia (composed of $c\bar{c}$ quarks) and bottomonia ($b\bar{b}$). The B_c^+ meson ($c\bar{b}$) is intermediate in binding energy between the J/ψ

($c\bar{c}$) and $\Upsilon(1S)$ ($b\bar{b}$) mesons, so its **dissociation** from the QGP screening of the heavy quark potential should be likewise intermediate. This hybrid state also offers a new point of view on the dependence of **energy loss** on the mass and colour charge of the traversing parton, as both the c and $\bar{b}$ quarks might undergo energy loss – these dependences, expected to be clearer at mid-p_T, are still ambiguous in the available measurements. Finally, the B_c^+ meson brings new light on the production of bound states from the **recombination of heavy quarks** from different nucleon-nucleon scatterings. This could explain the smaller J/ψ suppression at LHC than at RHIC, despite the higher QGP temperature at LHC. Up to 400 charm quarks roam freely in the QGP of the most central PbPb collisions at LHC, and can bind with uncorrelated c or b quarks. The B_c^+ meson has a very small cross section in pp collisions, so its production could be dramatically enhanced thanks to recombination, leading to $R_{AA} \gg 1$ values unseen for other hadrons.

Chapter 3 gives a brief history of CERN accelerators, a description of LHC experiments, in particular of the CMS detector, the global analysis strategy for observing B_c^+ mesons in heavy ion collisions with CMS, and details on the (MC-simulated) datasets and their normalisations. The analysed CMS data was taken in 2017 pp and 2018 PbPb collisions at a centre-of-mass energy of 5.02 TeV per nucleon pair, triggered by two muons with loose selections. The semi-leptonic decays $B_c^+ \to (J/\psi \to \mu^+\mu^-)\,\mu^+\,\nu_\mu$ are aimed for, despite the undetected neutrino, because their branching fraction is 20 times higher than the common fully reconstructed channel $B_c^+ \to (J/\psi \to \mu^+\mu^-)\,\pi^+$ [4]. A rapid analysis of the latter channel is lead; a mass peak is observed in pp, but the signal yields are insufficient in PbPb. The signal channel of interest hence results in a displaced vertex of three muons, with an opposite-sign dimuon whose mass is consistent with the J/ψ resonance. The signal trimuon mass distribution covers the $[3.2, 6.3]$ GeV range, so a major challenge of the analysis is to determine reliably the trimuon mass distributions of the background sources, which then allow for the signal extraction through a trimuon mass template fit.

The three main backgrounds and the samples used to describe them are detailed in chapter 4. The **fake J/ψ** events are the easiest to treat, as they can be emulated through the sidebands of the J/ψ dimuon mass peak. This sample is directly normalised by the sidebands data. The possible kinematic differences with the background under the J/ψ peak are accounted for by using the trimuon mass templates only from the higher or lower sideband instead of their sum. The **B decays** to a true J/ψ and a muon candidate (a misidentified charged hadron in most cases) are described with a MC sample. Only this background normalisation is left fully free in the fit. A systematic uncertainty accounts for other B_c decays than the signal one. Finally, the background from a **true J/ψ meson** combining with a **muon from a different decay** (i.e. not coming from the same displaced vertex) is described with an original data-driven **rotated J/ψ** method. The available MC simulations are indeed shown to largely fail to describe this background in pp. The displacement vector and the momentum of all J/ψ mesons in data are hence rotated, before being associated to a third muon candidate as in the signal region sample. Thirteen azimuthal rotation angles are used, with or without inverting rapidity. In PbPb, the associated muons are mostly uncorrelated with the J/ψ meson, so the distributions from all rotation angles are consistent and averaged, with a data-derived normalization. In pp, there are residual correlations between the J/ψ and the muon, for example when the two particles come from the same $b\bar{b}$ pair. This leads to different distributions for different rotation angles, which is accounted for by considering various mixes of these distributions. The control region at $m^{\mu\mu\mu} > 6.2$ GeV, containing only rotated J/ψ and J/ψ sidebands events, then fixes the normalisation in the fit procedure.

The signal selection is determined in chapter 5. To reach the observation of the B_c meson in PbPb considering the higher background and lower available nucleon-nucleon luminosity than in pp collisions, lowering the p_T acceptance threshold of muons in CMS is paramount. The B_c cross section indeed rises towards lower p_T regions, and recombined B_c mesons are expected at rather low p_T. The muon p_T threshold is hence lowered by matching it to the efficient region, depending on its rapidity and on whether it is required to fire the double-muon trigger. The resulting muon

acceptance limits were used in most low-p_{T} dimuon analyses in the heavy ions group – as was the software to select and build dimuon samples, that was augmented and maintained by the author. The results are quoted in two rapidity-dependent regions of the trimuon transverse momentum $p_{\mathrm{T}}^{\mu\mu\mu}$, following efficient regions, and in two centrality regions, integrated over kinematics.

Requirements are applied on the signal and the three background samples. The selection variables are the trimuon vertex fit probability, the significance of its displacement from the collision vertex, the angle between the trimuon momentum and the trimuon vertex displacement, the mass corrected for the momentum of the neutrino transverse to the $\mathrm{B_c}$ momentum, and the sum of the pseudo-angles between the three muon pairs. For the 5-6% of selected trimuons having two opposite-sign dimuons in the J/ψ peak or sidebands mass regions, two corresponding trimuon candidates are kept, weighted by the probability of the chosen dimuon to be a true J/ψ meson.

A boosted decision tree (BDT) is then trained on the selected background and simulated signal candidates. This combines the discriminating power of the five variables discussed above and of three sophisticated ones, including the p_{T} imbalance between J/ψ and the third muon, and the ratio of the pseudo-angles of J/ψ and of the other dimuon combinations. The BDT output variable is used to build signal- and background-enriched regions to be fitted – not for selection.

In chapter 6, a likelihood fit is performed in pp and PbPb collisions on the selected signal and background trimuon mass templates, simultaneously in three BDT bins, and in the two analysis bins ($p_{\mathrm{T}}^{\mu\mu\mu}$ or centrality) whose signal yields are hence extracted. The systematic uncertainties on the normalisation and shape of the background samples are implemented through nuisance parameters. The fitted mass distributions in PbPb integrated on the $p_{\mathrm{T}}^{\mu\mu\mu}$ bins are shown in Fig. 2. An uncertainty on the choice of fit method is also extracted, by varying the mass and bin limits and the treatment of the statistically-limited templates, and by using a BDT variable decorrelated from the mass. The significance of this first observation of $\mathrm{B_c}$ mesons in PbPb collisions is 6.8 standard deviations, considering the fit likelihood and the fit method uncertainty.

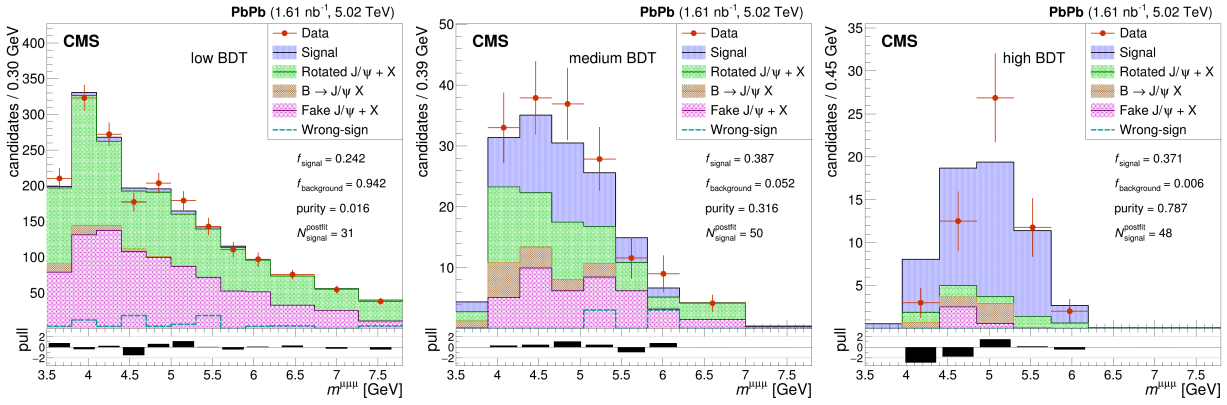

Figure 2: Template fit of the trimuon mass distributions in the three BDT bins in PbPb, integrated over the two studied kinematic regions.

The trimuon signal yields must then be corrected for the acceptance and efficiency of their triggering, reconstruction and selection, that are extracted in each analysis bin from the MC signal as explained in chapter 7. The single muon efficiencies in MC are weighted to those in data, estimated with a tag-an-probe method based on the J/ψ resonance. In pp, the tag-and-probe study is lead by the author and serves other dimuon analyses. The application of these corrections to the trimuons needs care, as only two muons need to trigger and pass tighter acceptance cuts.

The acceptance and efficiency of a signal trimuon strongly depend on its kinematic properties. As the studied kinematic regions are wide, and the p_{T} spectrum of $\mathrm{B_c}$ mesons is poorly known and simulated, an iterative procedure is built. The $p_{\mathrm{T}}^{\mu\mu\mu}$ spectrum in MC is first corrected to that measured in a first run of the analysis. The whole analysis is then re-run using now the corrected

MC, to determine a $p_{\mathrm{T}}^{\mu\mu\mu}$ spectrum with which the MC is corrected again, before extracting the final acceptance and efficiency. The related uncertainty exploits 1500 variations of the $p_{\mathrm{T}}^{\mu\mu\mu}$ spectrum within the uncertainties of its measurement. Each spectrum variation results in a different corrected 'toy' MC and associated acceptance and efficiency value. The RMS spread of the latter gives the uncertainty in p_{T}-integrated bins. The uncertainty in p_{T} bins is the RMS of the corrected yields from each toy MC, to account for the correlations of all uncertainty sources.

Chapter 8 summarises the uncertainty sources and how their bin-to-bin correlations are estimated. Chapter 9 presents the pp and PbPb cross sections and the $R_{\mathrm{PbPb}}(\mathrm{B_c^+})$ measurements, and compares R_{PbPb} to theoretical predictions and measurements of other hadrons. The pp cross section shows that BCVEGPY [5], specialised in simulating the production of $\mathrm{B_c}$ states, overestimates the high-p_{T} spectrum slope. The measured $R_{\mathrm{PbPb}}(\mathrm{B_c^+})$ shows no dependence as a function of the collision centrality. However, at low p_{T} it is higher than at high p_{T} and than 1, with respective significances of 1.8 and 1.2 standard deviations, which favours a softening of the p_{T} spectrum and suggests a large enhancement at lower p_{T} values than those accessible with CMS. With much higher significance, R_{PbPb} stands higher for $\mathrm{B_c}$ than for all other hadrons, except the $\mathrm{B_s^0}$ meson (see Fig. 3). Theoretical $R_{\mathrm{PbPb}}(\mathrm{B_c^+})$ predictions in the studied kinematic range based on the model of Ref. [6] are an order of magnitude lower than our measurement (see Fig. 3). All these comparisons suggest that a production mechanism compensates the expected suppression of heavy quark bound states. Heavy quark recombination is the main proposed interpretation of such enhancement; future measurements with more data, and hopefully at lower p_{T}, will unambiguously show the existence of recombination, especially if $R_{\mathrm{PbPb}}(\mathrm{B_c^+}) > 1$ values are confirmed, and will help discriminate among the available recombination models. This analysis opens the way for these measurements; it is also only the second one in the CMS heavy ion group to partially blind the PbPb data before finalising all analysis strategies (to avoid human biases in the choices thereof) and to use a sophisticated simultaneous likelihood fit.

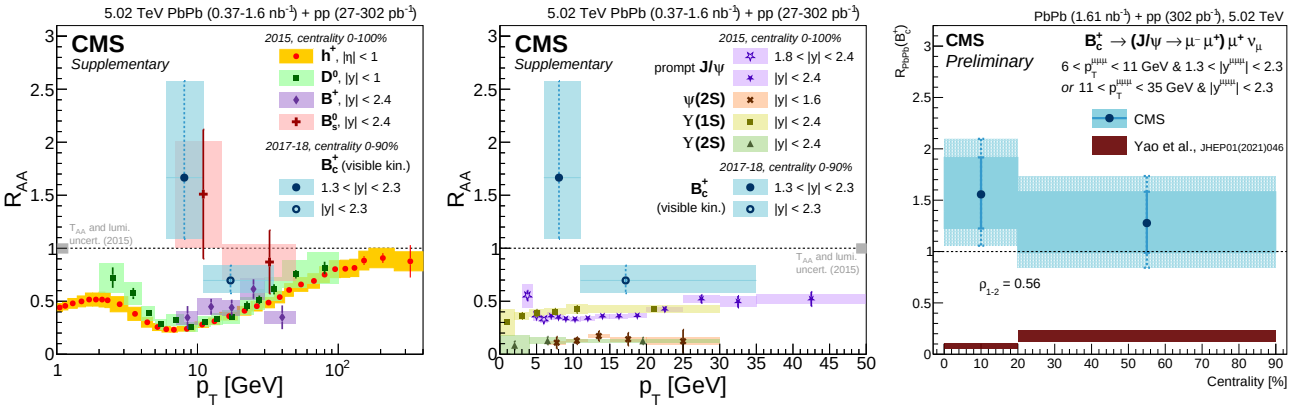

Figure 3: Nuclear modification factor of the $\mathrm{B_c}$ meson, compared to that of other hadrons and to theoretical predictions. *Left:* p_{T} dependence compared to that of other open heavy flavour mesons. *Middle:* idem with hidden heavy flavour mesons. *Right:* centrality dependence compared to a prediction based on Ref. [6].

The second part of the thesis develops on a model of medium-induced radiative energy loss of partons at high p_{T}, where it is expected to be the dominant QGP effect modifying hadron production. Chapter 10 describes the BDMPS emitted gluon spectrum in the QGP [7], and the model based on it that predicts a universal p_{T} shape of the R_{AA} of high-p_{T} hadrons; R_{AA} hence depends only on a typical energy loss value [2], and on the fitted slope n of the p_{T} spectrum in pp. The original model tested this $R_{\mathrm{AA}}(p_{\mathrm{T}})$ scaling on a few measurements of hadrons at $p_{\mathrm{T}} \gtrsim 10\,\mathrm{GeV}$, allowing for the extraction of the mean energy loss values $\langle\varepsilon\rangle$ of partons times their mean fragmentation $\langle z\rangle$ into the observed hadrons.

This scaling is furthermore confirmed in chapter 11 with 62 gathered sets of hadron R_{AA}

measurements in very different conditions. These LHC and RHIC measurements concern 3 hadron species (light hadrons and D and J/ψ mesons), 3 collision systems (PbPb, xenon-xenon, and gold-gold), 4 center-of-mass energies (from 0.2 to 5.44 TeV), many centrality ranges, and 4 experiments. The scaling of most light hadron R_{AA} measurements is shown in Fig. 4 (*left*). Each set results in a fitted value of $\langle\varepsilon\rangle\langle z\rangle$, and realistic uncertainties, including systematic sources, are calculated.

The main contribution of this study, also in chapter 11, is to demonstrate that these energy loss values scale with the density, the path length L, and the transverse area $A_\perp$ of the medium, and to constrain the expansion properties of the medium therefrom. This scaling makes use of the equivalent transport coefficient $\langle\hat{q}\rangle \propto n_0(\tau/\tau_0)^\alpha$ for an expanding medium [8], where α characterises the expansion and equals 1 for a longitudinal 'Bjorken' expansion. This leads to a dependence $\langle\varepsilon\rangle \propto L^{2-\alpha}\ \frac{\mathrm{d}N_{\mathrm{ch}}}{\mathrm{d}\eta}/A_\perp$, at odds with the $\varepsilon \propto \hat{q}L^2$ standard dependence in a static medium.

The multiplicity of charged particles, proportional to the medium density, is taken from measurements in each studied system. The mean path length of partons in the medium and its transverse area require a Glauber model to describe the geometry of the collision. Four models are tested: an existing MC Glauber with tabulated values [9], a simple case where nuclei are hard spheres and the medium density is constant, and two complete and custom optical Glauber models, with hard-sphere or Woods-Saxons nucleus densities. As shown in Fig. 4 (*right*), the energy loss and computed path length and area values for the many different measured systems indeed scale as predicted, and the corresponding fit provides values of α and of the proportionality coefficient. The first is found consistent with a longitudinal medium expansion ($\alpha = 1.00 \pm 0.09$), while the latter constrains the product $\alpha_S^3\, C_R\, \langle z\rangle$, where C_R is the colour factor of the traversing parton.

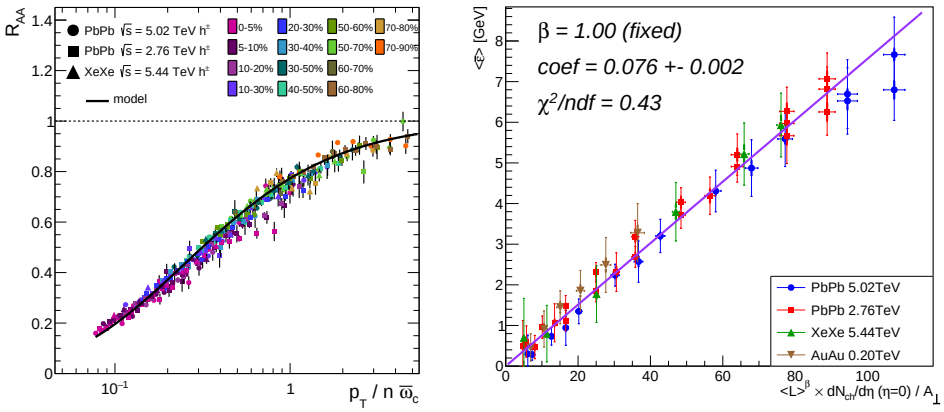

Figure 4: *Left:* Scaling of many charged hadron R_{AA} measurements with the predicted p_{T} dependence. *Right:* scaling of the energy loss values in very different systems with the path length in the medium and the particle multiplicity.

Finally, chapter 12 discusses some limitations of the model, notably the independence of various involved integrals and the influence of the nature of the traversing parton. Possible predictions of the light hadron R_{AA} in oxygen-oxygen collisions and of the azimuthal asymmetry coefficient v_2 of hadrons at high p_{T} are also discussed.

[1] CMS Collaboration, arXiv:**2201.02659**, 2022.
[2] F. Arleo, Phys. Rev. Lett., **119(6)**, 062302, 2017.
[3] F. Arleo and G. Falmagne, PoS, **HardProbes2018**, 075, 2019.
[4] LHCb Collaboration, Phys. Rev. D, **90**, 032009, 2014.
[5] C.-H. Chang, X.-Y. Wang, and X.-G. Wu, Comput. Phys. Commun., **197**, 335–338, 2015.
[6] X. Yao, W. Ke, Y. Xu, S. A. Bass, and B. Müller, JHEP, **21**, 046, 2020.
[7] R. Baier et al., Nucl. Phys. B, **483**, 291–320, 1997.
[8] C. A. Salgado and U. A. Wiedemann, Phys. Rev. Lett., **89**, 092303, 2002.
[9] C. Loizides et al., Phys. Rev. C, **97(5)**, 054910, 2018. [Erratum: Phys.Rev.C 99, 019901].